Freshwater Biology

Freshwater Biology (2010) **55,** 1658–1673 doi:10.1111/j.1365-2427.2010.02400.x

Differentiating aquatic plant communities in a eutrophic river using hyperspectral and multispectral remote sensing

YONG Q. TIAN*, QIAN YU†, MARC J. ZIMMERMAN‡, SUZANNE FLINT§ AND MARCUS C. WALDRON‡

*Department of Environmental, Earth and Ocean Sci., Univ. of Massachusetts Boston, Boston, MA, U.S.A.

†Department of Geosciences, University of Massachusetts-Amherst, MA, U.S.A.

‡USGS MA-RI Water Science Center, Northborough, MA, U.S.A.

§Organization for the Assabet River, Concord, MA, U.S.A.

SUMMARY

1. This study evaluates the efficacy of remote sensing technology to monitor species composition, areal extent and density of aquatic plants (macrophytes and filamentous algae) in impoundments where their presence may violate water-quality standards.
2. Multispectral satellite (IKONOS) images and more than 500 *in situ* hyperspectral samples were acquired to map aquatic plant distributions. By analyzing field measurements, we created a library of hyperspectral signatures for a variety of aquatic plant species, associations and densities. We also used three vegetation indices. Normalized Difference Vegetation Index (NDVI), near-infrared (NIR)-Green Angle Index (NGAI) and normalized water absorption depth (D_H), at wavelengths 554, 680, 820 and 977 nm to differentiate among aquatic plant species composition, areal density and thickness in cases where hyperspectral analysis yielded potentially ambiguous interpretations.
3. We compared the NDVI derived from IKONOS imagery with the *in situ*, hyperspectral-derived NDVI. The IKONOS-based images were also compared to data obtained through routine visual observations. Our results confirmed that aquatic species composition alters spectral signatures and affects the accuracy of remote sensing of aquatic plant density. The results also demonstrated that the NGAI has apparent advantages in estimating density over the NDVI and the D_H.
4. In the feature space of the three indices, 3D scatter plot analysis revealed that hyperspectral data can differentiate several aquatic plant associations. High-resolution multispectral imagery provided useful information to distinguish among biophysical aquatic plant characteristics. Classification analysis indicated that using satellite imagery to assess *Lemna* coverage yielded an overall agreement of 79% with visual observations and >90% agreement for the densest aquatic plant coverages.
5. Interpretation of biophysical parameters derived from high-resolution satellite or airborne imagery should prove to be a valuable approach for assessing the effectiveness of management practices for controlling aquatic plant growth in inland waters, as well as for routine monitoring of aquatic plants in lakes and suitable lentic environments.

Keywords: aquatic macrophytes, hyperspectral, multispectral, remote sensing

Correspondence: Yong Q. Tian, Department of Environmental, Earth and Ocean Sci., Univ. of Massachusetts Boston, Boston, MA, U.S.A. E-mail: yong.tian@umb.edu

Introduction

Aquatic vegetation has long been used as an indicator of nutrient loading in river ecosystems (Junk, 1997; Marion & Paillisson, 2003), but estimating the extent and biomass of aquatic plant growth is not a trivial task. High-resolution, multispectral remote sensing technology offers a potentially convenient means of assessing aquatic plant growth in a synoptic view (Silva *et al*., 2008). In recent years, studies applying remote sensing of aquatic vegetation in river environments have become more common (Penuelas *et al*., 1993; Jakubauskas *et al*., 2000; Nelson, Cheruvelil & Soranno, 2006; Nezlin, Kamer & Stein, 2007). However, the results of these studies were primarily applied to monitoring of specific aquatic plant species; for example, Jakubauskas *et al*. (2000) remotely assessed the density of *Nuphar polysepala*, a perennial aquatic plant with large leaves and spongy rhizome.

Remote sensing of aquatic plant communities presents different challenges from the more extensively studied terrestrial communities. Floating and rooted macrophytes, and submerged algae, differ substantially from terrestrial plants in concentrations of leaf pigments, morphology and water content – biophysical characteristics that determine reflectance and absorption in visible and near-infrared wavelengths. In addition, water movements mix floating plants, thereby continuously changing reflectance and absorption characteristics such as leaf angle, species mixture and layer density. Therefore, in this study, we sought to determine the extent to which aquatic plant species composition affects the use of remote sensing data to evaluate aquatic plant density and thickness for future applications in determining biomass. By analyzing a large set of *in situ* hyperspectral measurements of *Lemna*-dominated aquatic plant associations, we created a library of hyperspectral signatures for a variety of plant species and associations. Based on the improved understanding of those spectral responses, we examined three vegetation indices at wavelengths in the visible and NIR regions for use in remote sensing of aquatic plant species composition, density and thickness. We attempted to determine whether the Normalized Difference Vegetation Index (NDVI) derived from IKONOS imagery could substitute for the *in situ* hyperspectral-derived NDVI for the assessment of aquatic plant distribution. Results from IKONOS imagery were compared to data obtained through routine visual observations.

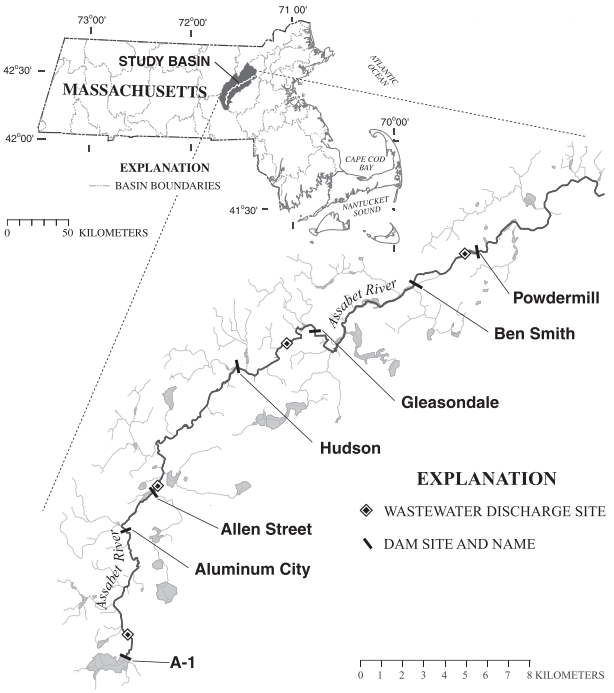

Fig. 1 Locations of wastewater discharges and major dams impounding the Assabet River in central Massachusetts.

Methods

The Ben Smith and Hudson impoundments of the Assabet River, in east-central Massachusetts, served as the study area (Fig. 1); maximum depth in the impoundments is approximately 4.5 m. The Assabet River, part of a federally designated Wild and Scenic River, flows for 50 km from its headwaters at the A-1 impoundment in Westborough to its confluence with the Sudbury River, forming the Concord River, in Concord. The river's elevation drops about 100 m along its length and nine dams create long, relatively shallow impoundments. Four publicly owned treatment works (POTWs) have permits to discharge a total of approximately 57 000 m^3 d^{-1} into the river; three POTWs are upstream from the study area and one is downstream. These discharges have been identified as the primary sources of the nutrients responsible for eutrophic conditions throughout the Assabet River. The visible effect of these eutrophic conditions is the heavy growth of aquatic plants that

Table 1 Description of six primary aquatic plant distributions in the Ben Smith and Hudson impoundments of the Assabet River

Brief descriptor used in text	General description
Lemna	Mixture of *Lemna minor* (*c.* 70%) *and Wolffia sp.*, (probably *W. columbiana*) at various per cent areal coverages over generally clear water
Lemna in a thin layer	*Lemna/Wolffia* mixture, 100% areal coverage, in a thin layer (0.1–0.2 cm thick)
Lemna in a moderate layer	*Lemna/Wolffia* mixture, 100% areal coverage, in a moderate layer (0.2–0.5 cm thick)
Lemna in a thick layer	*Lemna/Wolffia* mixture, 100% areal coverage, in a thick layer (0.5–1.0 cm thick)
Wolffia/Lemna	*Wolffia/Lemna minor* mixture with *Wolffia* dominant (*c.* 65%)
Potamogeton	*Potamogeton mixed with Lemna/Wolffia*
Lemna with algae	*Lemna/Wolffia* with mats of green algae, primarily *Hydrodictyon* and *Spirogyra* that may include decaying or dead plant material
Ceratophyllum	*Ceratophyllum*, a submerged aquatic macrophyte attached to the bottom and generally covered with epiphytic algae in relatively shallow water (<0.5 m); may be mixed with *Elodea sp.*
Clear water	Open water, generally >1 m deep, with no clumps of aquatic plants

is especially apparent near dams and channel constrictions, such as bridges.

The dominant floating plants in the Assabet River impoundments are *Lemna minor*, *Wolffia sp.* (probably *W. columbiana*), *Hydrodictyon sp.* and *Potamogeton natans* (Table 1). Other common aquatic plants include *Elodea canadensis*, *Ceratophyllum demersum*, *Cabomba caroliniana* and *Trapa natans*.

In situ *hyperspectral data collection*

Spectral measurements of aquatic plants were collected in the Hudson and Ben Smith impoundments with a FieldSpec 3 spectroradiometer (Analytical Spectral Devices (ASD), Boulder, CO, U.S.A.). The instrument uses three separate detectors spanning the visible and near-infrared (VNIR, 350–1050 nm) and shortwave infrared (SWIR1, 1000–1800 nm, and SWIR2, 1800–2500 nm) spectra. After re-sampling, the spectroradiometer produces spectral reflectance values for every 1 nm in wavelength at the range of 350–2500 nm, creating a 2150-band spectrum for each sample point (ASD Inc., 2008).

In situ hyperspectral data were acquired from 10 : 26 to 14 : 11 on 12 August 2007 and from 11 : 00 to 14 : 36 on 15 September 2007 when the extent of aquatic plant growth was at its annual maximum. Hyperspectral measurements (samples) were made simultaneously with GPS positions. To avoid boat shadow effects at all orientations, the spectroradiometer with a 5-m fibre-optic cable was mounted to allow the sensor probe to reach out more than 3 m from the boat. The sensor probe, with its 25° field of view, was set about 1.5 m above the water surface. To maintain consistent sampling while the boat navigated in different orientations, the sensor angle was set to point perpendicularly at the water surface (nadir direction). We conducted instrument optimizations at the outset and during hyperspectral data acquisition. The sensor was calibrated every 10 min, or following changes in cloud cover, by taking white reference measurements with a Spectralon (Labsphere, North Sutton, NH, U.S.A.) white reference panel.

A total of 579 *in situ* hyperspectral measurements (samples) were made corresponding to the six most apparent aquatic plant distributions or associations (Table 1). Data for two of the most important regulatory concerns – *Lemna* areal coverage and layer thickness – accounted for a majority of the samples (328). The distribution among the other associations includes 50 samples of *Lemna* with algae, 102 samples for *Ceratophyllum*, 36 samples for floating-leaved *Potamogeton* and 63 samples for *Wolffia/Lemna* mixtures where *Wolffia* was the predominant species. In the sections sampled, *Lemna* areal coverage ranged from 0 to 100%. For 100% *Lemna* coverage (166 samples), the spectral responses can differ depending on the accumulation of layers of *Lemna* caused by wind and currents. Based on our field observations, we categorized the thicknesses of these layers into three groups: thin (0.1–0.2 cm), moderate (0.2–0.5 cm) and thick (0.5–1.0 cm).

Vegetation indices

Three vegetation indices were examined for quantifying aquatic plant areal coverage and layer thicknesses

and for identifying species associations: NDVI, NGAI and D_H. Each index has unique characteristics that make it useful in the identification of aquatic plants. Some modifications were made to the indices to apply them appropriately to aquatic conditions in the Assabet River system.

The NDVI, a well-known and widely used vegetation index developed by Rouse *et al.* (1974), is based on the contrast between the maximum absorption in the red band because of chlorophyll pigments and the maximum reflectance in NIR caused by leaf cellular structure. The NDVI has proved effective in identifying biophysical parameters of dense and multilayered canopies (Lillesaeter, 1982; Baret & Guyot, 1991). Using narrow, hyperspectral bands for aquatic vegetation, the NDVI was calculated as follows:

$$\mathrm{NDVI} = (\rho_{820} - \rho_{680})/(\rho_{820} + \rho_{680}) \quad (1)$$

where ρ_λ is the reflectance at the wavelength λ (nm).

The NGAI is an adaptation of an angle index first introduced by Palacios-Orueta *et al.* (2006) and a later Shortwave Angle Slope Index (SASI) proposed by Khanna *et al.* (2007). These latter angle indices parameterize the general shape of the spectrum by measuring the angles formed by combining the NIR and two MODIS (Moderate Resolution Imaging Spectroradiometer) bands of SWIR. In terrestrial systems, these angle indices are effective in tracking soil moisture and discriminating soil and vegetation (Khanna *et al.*, 2007; Numata *et al.*, 2008). The NGAI is applied here to assess aquatic plant characteristics derived from hyperspectral data. The traditional angle indices were modified by using three bands: NIR_1 (820 nm), NIR_2 (977 nm) and green (554 nm) (Fig. 2). The resulting angle index, A_{NIR} (in radians), is calculated as

$$A_{\mathrm{NIR}} = \cos^{-1}\left[\frac{a^2 + b^2 + c^2}{2ab}\right] \quad (2)$$

where a, b and c are Euclidian distances between vertices at three bands.

Angle indices are commonly normalized to reduce the influence of sensor–solar geometry. Khanna *et al.* (2007) indicated that the slope of a line adjacent to the angle A_{NIR} performs better in most cases than the common normalized form. Therefore, we used the slope of the line connecting the vertices between ρ_g and ρ_{NIR1} (eqn 3) and, then, normalized the NGAI (eqn 4)

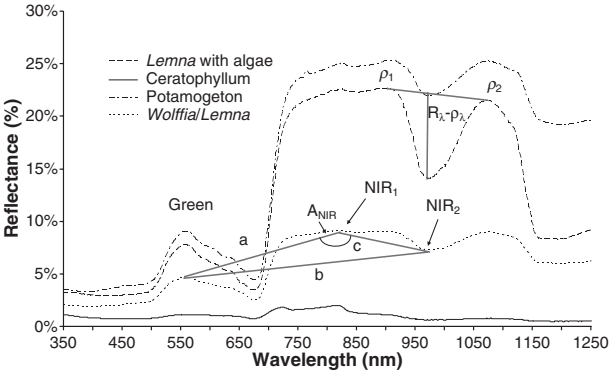

Fig. 2 Spectral responses to four aquatic plant distributions. Red lines illustrate elements of the NIR and Green Angle Index and the continuum removal function.

$$\mathrm{Slope} = \rho_{\mathrm{NIR1}} - \rho_g + 0.03 \quad (3)$$

$$\mathrm{NGAI} = \mathrm{Slope} * \mathrm{A_{NIR}} \quad (4)$$

where slope is the difference between spectral reflectance at the NIR_1 band and the green band (554 nm) plus 0.03. The constant 0.03 is added to avoid negative values when the data primarily represent open water conditions. The NGAI value in radians was calculated for all samples and was adopted as a parameter for estimating aquatic plant areal coverage and for identifying species compositions.

The D_H describes a feature relating the common baseline to spectral reflectance at the wavelength where the local minimum forms. Previous research has used the absorption area instead of depth as part of a continuum removal method (Clark & Roush, 1984; Khanna *et al.*, 2007). The absorption area is the product of absorption depth and the width of absorption which is the full wavelength width at half absorption depth (Numata *et al.*, 2008). However, in this study, the three wavelengths controlling the absorption area of the spectral curve are similar for all samples (λ_1 is about 915 nm; λ_2 is about 1075 nm; and λ is about 977 nm), which means the absorption widths show little difference between samples. We considered D_H as the index of the continuum without including the width and used D_H to represent absorption characteristics of aquatic plants and species composition.

A number of applications have successfully used continuum removal to determine absorption features for terrestrial biophysical parameters, such as leaf

biochemistry (Kokaly & Clark, 1999), forest leaf area index (Pu *et al.*, 2003) and pasture biomass (Numata *et al.*, 2008). Continuum removal is a mathematical function used to isolate a particular absorption feature for analysis of a spectrum (Clark & Roush, 1984). D_H was applied to one spectral absorption region between 915 nm and 1075 nm. The depth of the spectral absorption at about 977 nm was calculated using the continuum removal function as a common baseline between the two local spectral maxima (ρ_1 and ρ_2) in the absorption region (Fig. 2). The following linear equation represents the common baseline function, or continuum, R_λ, at wavelength λ, which varies between λ_1 and λ_2

$$R_\lambda = \frac{\rho_{\lambda_2} - \rho_{\lambda_1}}{\lambda_2 - \lambda_1} * (\lambda - \lambda_1) + \rho_{\lambda_1} \quad (5)$$

where $\rho_{\lambda_1}$is reflectance at band λ_1, which has a local maximum at 915 nm ($\lambda_1 = 915$), and ρ_{λ_2} is reflectance at band λ_2, with a local maximum around at 1075 nm ($\lambda_2 = 1075$). The local minimum (ρ_λ) in this case occurs when $\lambda = 977$ nm. Therefore, D_H, at the local minimum, can be calculated as

$$D_H = \frac{R_\lambda - \rho_\lambda}{R_\lambda} \quad (6)$$

IKONOS data acquisition and pre-processing

Aquatic vegetation characteristics were assessed from IKONOS imagery acquired for the Ben Smith impoundment in the Assabet River on 15 August 2007. The *in situ* measurements were used to develop suitable spectral indices for distinguishing among aquatic plant communities and density, but not for correlating the classifications according to their spatial locations.

Pan-sharpening and atmospheric corrections were conducted before classification. Atmospheric conditions for the IKONOS images were corrected with an empirical line calibration (ELC) method (Jensen, 2007). *In situ* spectral reflectances of a sand trap in a nearby golf course and of deep, clear water areas of the impoundments served as bright and dark objects for calibrating satellite imagery data. The bright and dark pixels on the same objects were identified on the IKONOS images using GPS locations. The paired image digital number and field spectral reflectance were used to fit the linear regression model. Then, the model was applied to the entire image, converting digital values to reflectance and reducing errors introduced by atmospheric conditions.

IKONOS 4-band, multispectral images at 4-m resolution were transformed to 1-m resolution by panchromatic band referencing using a four-step, principal component spectral sharpening method (PC Spectral Sharpening). The first step was a PC transformation of the multispectral data. Next, the panchromatic band was scaled to match PC band 1 and then replaced it. In the third step, an inverse transform was performed on the newly combined, multispectral images. Finally, the resulting multispectral data were resampled to the 1-m panchromatic pixel size.

Field surveys of biophysical measurements

Data from routine visual surveys of aquatic plants from the riverbanks were used to corroborate the IKONOS image classification results for the Ben Smith impoundment. The survey was performed as part of a U.S. Geological Survey monitoring study of aquatic plant growth in sections of the Assabet River where the accumulation of aquatic plants exceeds Massachusetts water-quality standards. A grid, comprised of irregularly shaped cells and based on a series of transects approximately perpendicular to midstream, was established, and observations were made from several vantage points. Transects and observation points were selected to adequately map the distribution of aquatic plants in sections of the impoundments. A routine, visual survey was conducted on 16 August 2007, 1 day after IKONOS satellite imagery collection. Aquatic plant (*Lemna*) coverage, without regard to layer thickness, in each cell was ranked on a scale of 0–4 (0 = no plants observed, 1 = 1–25%, 2 = 26–50%, 3 = 51–75% and 4 = 76–100%) in accordance with protocols of the Massachusetts Department of Environmental Protection. The field-observation data were transferred to a Geographic Information System.

Results

Hyperspectral responses to aquatic plants in various distribution scenarios

Average spectral reflectance across wavelengths 350–2500 nm in response to *Lemna* areal coverages of 0–100% and three thickness levels (for 100% areal

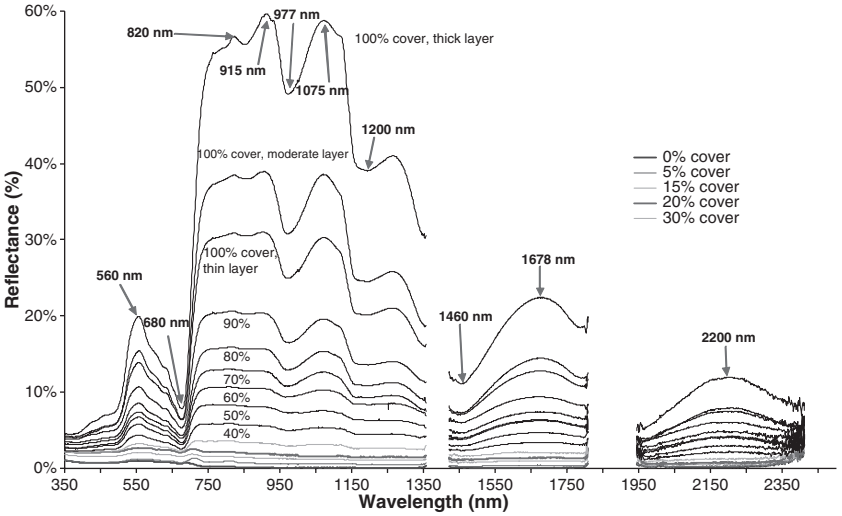

Fig. 3 Hyperspectral responses to *Lemna* areal coverage and layer thickness.

coverage only) indicate substantially greater NIR reflectance for dense areal coverages and thick-layered assemblages (Fig. 3). Since water absorbs strongly at wavelengths from approximately 1300–2500 nm (Curcio & Petty, 1951; Jacquemoud & Ustin, 2003), differences in reflectance in the short-wavelength infrared (SWIR) range (1450–1800 nm, and 1950–2350 nm) are effectively imperceptible for areas of <30% coverage. Overall reflectance in the 350–2500 nm region was greater with increasing per cent coverage and with increasing layer thickness, trending most sharply upward between 700 and 915 nm. At the same time, the depth of the water absorption features centred at wavelengths 977 and 1200 nm increased, creating distinctive features of the *Lemna* signature.

Even given the same areal coverage, major aquatic plant associations in the Assabet River have markedly different spectral responses (Fig. 4). The performance of remote sensing of submerged plants depends both on depth of the top of the vegetation and on turbidity. Although turbidity was not measured directly, total suspended solids (which contribute to turbidity) samples were collected on 18 August 2007. Concentrations of total suspended solids at sites upstream and downstream of the sampling areas were quite low, ranging from <1 mg/L to 3 mg/L.

The spectral signatures of *Potamogeton* are also distinct at green and NIR wavelengths (Fig. 4c). Although the shapes of their spectral curves are similar to *Lemna* for 100% coverages, their scales differ. The spectral reflectance of *Potamogeton* at 100% coverage is comparable to *Lemna* at 95%. *Potamogeton* usually has the thickness of one thin broad leaf whose internal structure determines the lower reflectance across the VNIR region. Because of the distinct R/NIR reflectance ratio, the NDVI should be able to distinguish *Potamogeton* from *Lemna*.

Reflectance characteristics of *Wolffia/Lemna* across VNIR bands may be as much as 50% less than the floating leaves of *Potamogeton* (Fig. 4c,d). Since *Lemna* and *Wolffia* generally occur in mixtures of various proportions, it can be difficult to use remote sensing to differentiate the individual areal coverage and layer thickness of these small aquatic macrophytes. Their biological features, colour and distribution as low-density specks result in relatively low reflectance in all wavelengths. In addition, *Wolffia*-dominated mixtures (*Wolffia/Lemna*) absorb strongly at wavelengths centred at 977 nm.

Resolving challenging classification scenarios with hyperspectral data

Complex, or potentially ambiguous, hyperspectral responses were identified in four scenarios describing *Lemna* coverage and aquatic plant associations. First, 90% *Lemna* areal coverage has a spectral signature similar to *Lemna* with algae (Fig. 5a). Second, submerged plants and low-density *Lemna* (areal coverage from 0 to 15%) have similar signatures (Fig. 5b). Third, *Potamogeton* and dense *Lemna* with algae in

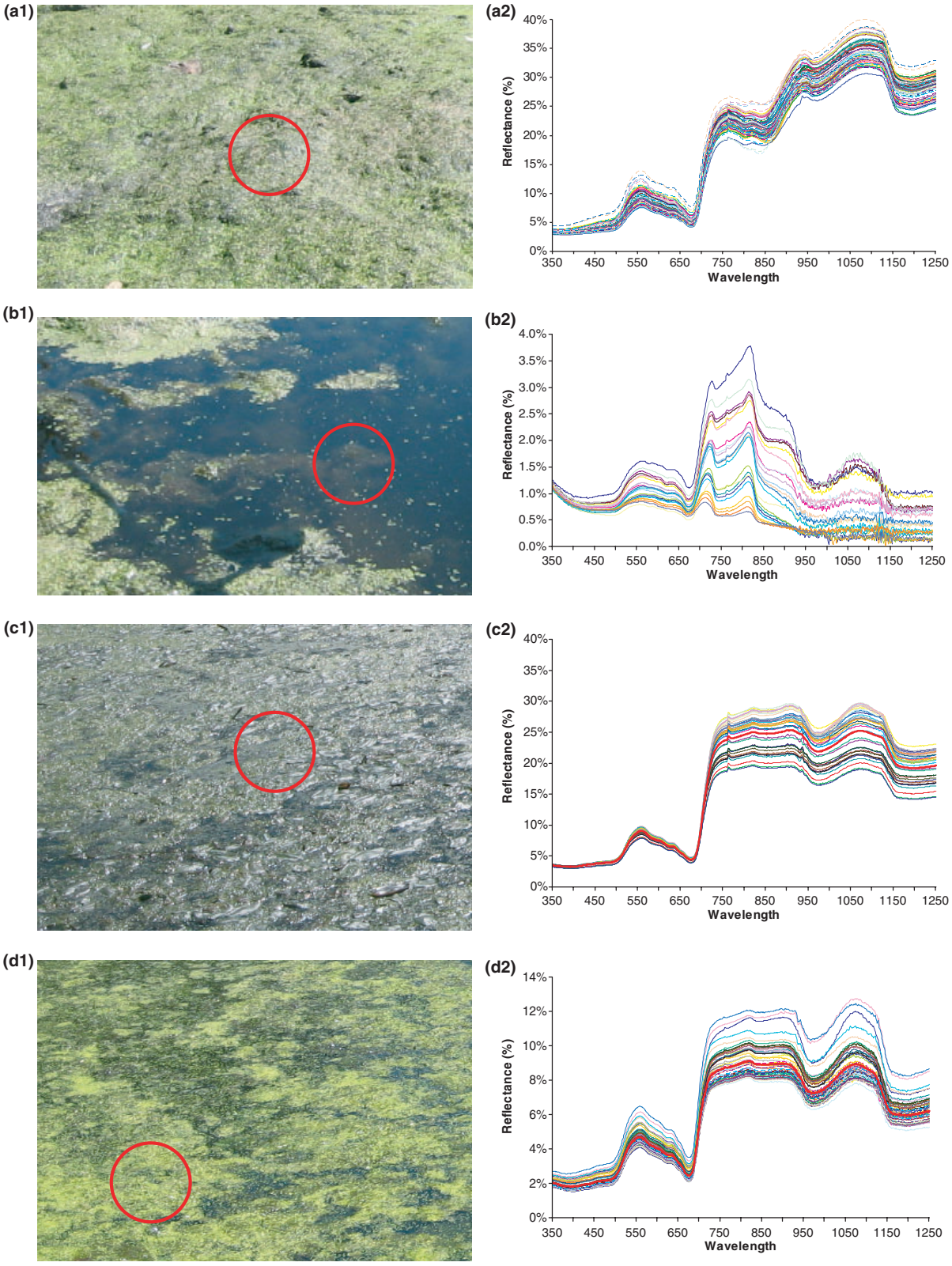

Fig. 4 Hyperspectral responses to major aquatic plant associations: (a) *Lemna* with algae; (b) *Ceratophyllum;* (c) *Potamogeton;* (d) *Wolffia/Lemna*. Reflectance value scale in b and d is different from a and c.

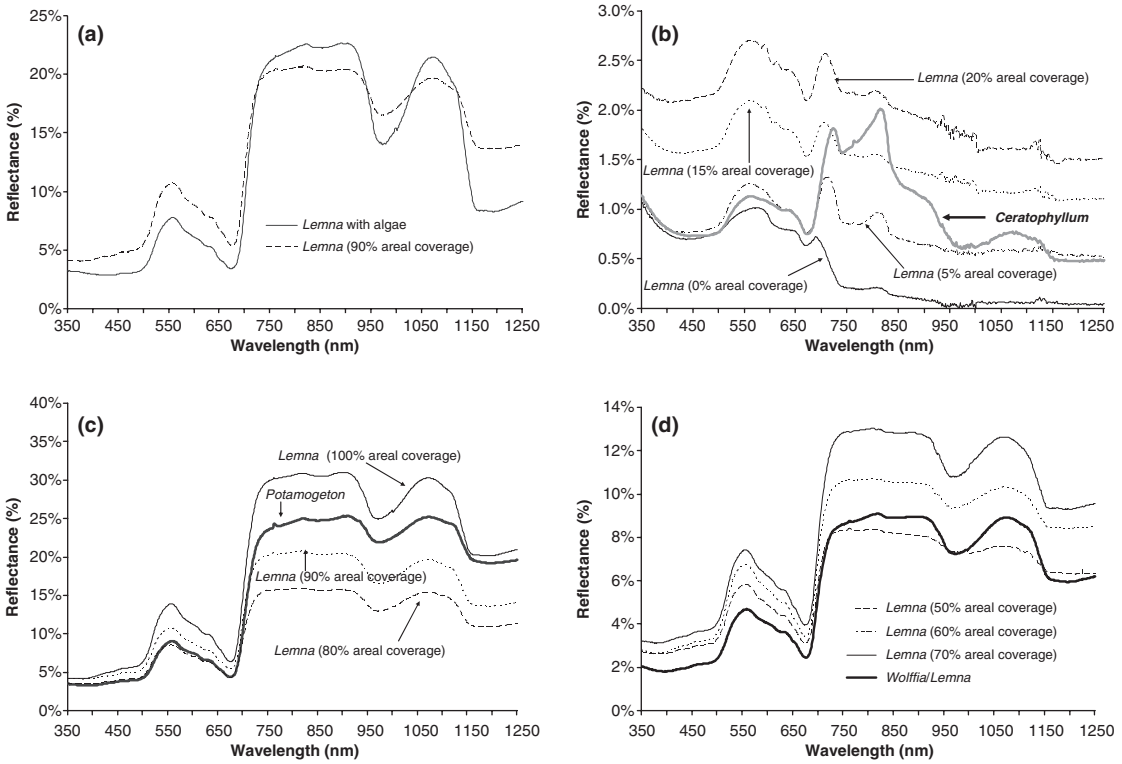

Fig. 5 Complex, or ambiguous, spectral responses: (a) *Lemna* (90% areal coverage) and *Lemna* with algae; (b) *Ceratophyllum* and *Lemna* (5–20% areal coverage); (c) *Potamogeton* and *Lemna* (90–100% areal coverage); (d) *Wolffia/Lemna* (50–70% areal coverage). Reflectance scales vary in a through d.

mats (areal coverage from 90 to 100%; Fig. 5c) have similar reflectance ranges and signature curves. Finally, the *Wolffia*-dominated *Wolffia/Lemna* association and *Lemna* at 50–60% areal coverage (Fig. 5d) are spectrally similar except that the spectral reflectance for *Wolffia/Lemna* shows a rising slope between 750 and 915 nm.

Use of satellite imagery for interpreting aquatic plant thickness and associations

The four spectral bands from an IKONOS image acquired for the Ben Smith impoundment were processed with atmospheric correction and pan-sharpening followed by unsupervised classification. With the widely used Iterative Self-Organizing Data Analysis Technique (ISODATA) (ERDAS, 2003; Rees, Williams & Vitebsky, 2003; Stow *et al.*, 2003), the image was initially classified into 10 groups. Using the spatial patterns of each class observed in the visual field assessment, we condensed the 10 original groups into six similar to those identified in the hyperspectral analyses: open water, thin, moderate and thick layers of *Lemna*, *Potamogeton* and *Lemna* with algae. To confirm that the groups generated by the unsupervised classification were correctly identified, we compared the mean NDVI for each of the five aquatic plant classes from the unsupervised classification with the mean NDVI derived from the *in situ* hyperspectral measurements (Fig. 6). Overall, the NDVI derived from IKONOS data and the NDVI derived from *in situ* hyperspectral data for the five classes were similar.

Estimating Lemna *coverage with vegetative indices*

Two vegetation indices, NDVI and NGAI, were compared to see which correlated best with *Lemna* areal coverage and layer thickness. Statistical analysis showed that NDVI and NGAI both performed well in predicting *Lemna* coverage (Fig. 7). Using an exponential function (eqn 7), the NDVI explained 77% of *Lemna* coverage (C_p). Since the NDVI for water is negative, the constant 0.15 was used to shift the NDVI

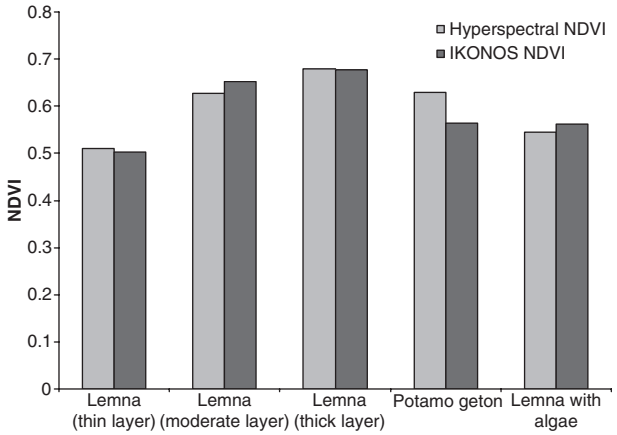

Fig. 6 Bar charts comparing NDVI derived from *in-situ* hyperspectral data and IKONOS multispectral imagery.

values to avoid having a negative value in the exponential function.

$$C_p = f(\mathrm{NDVI} + 0.15) = 0.078e^{3.136(\mathrm{NDVI}+0.15)} \quad (7)$$

Using the NGAI with the logarithmic function (eqn 8) improved estimates of *Lemna* areal coverage to 95%.

$$C_p = f(\mathrm{NGAI}) = 0.4312\ln(\mathrm{NGAI}) + 1.5522 \quad (8)$$

Identifying aquatic plant thickness and species associations

Projected in a feature space, the three vegetation indices can provide the means for visually distinguishing seven classes of aquatic plant distributions: three thickness classes of the *Lemna* association, submerged macrophytes (primarily *Ceratophyllum*), *Potamogeton*, *Lemna* mixed with floating algae (*Hydrodictyon*) and *Wolffia/Lemna* (Fig. 8). The NGAI was positively related to *Lemna* thickness and to many of these species composition scenarios. Two data clusters (lower left in Fig. 8a) represent *Wolffia/Lemna* and *Ceratophyllum*. Although the *Wolffia/Lemna* association had a stronger reflectance across the spectrum than *Ceratophyllum*, both plant types had similar ranges of low NGAI and NDVI values. In a like manner, *Potamogeton* and *Lemna* in a moderate layer have similar ranges of NDVI and D_H values that preclude their differentiation on the basis of those two indices. For each of these latter two sets of data, a third index is needed to distinguish the associations.

Resolving challenging scenarios with vegetative indices

The three vegetation indices can be used effectively to resolve the complex scenarios noted previously. The NDVI and the NGAI can each differentiate between *Lemna* mixed with floating algae and dense *Lemna* (90% areal coverage; Figs 5 & 9a). The NDVI can differentiate submerged *Ceratophyllum* from low areal density *Lemna*, given the distinctly different R/NIR reflectance ratios (Figs 5b & 9b). The combination of the NDVI and NGAI is effective for separating *Potamogeton* from highly dense *Lemna* concentrations (Fig. 9c). Separating *Wolffia/Lemna* from moderate-density *Lemna* (50–60% areal coverage) requires both the NDVI and the NGAI (Fig. 9d). Overall, at high areal coverages, *Lemna* (90–100%) is more easily classified by the NDVI and the NGAI than at moderate coverages (Fig. 9b–d).

Comparison of satellite imagery and visual observations

Our results show that the hyperspectral NDVI alone is capable of classifying many of the aquatic vegetation scenarios described here, such as *Lemna* areal coverage (Fig. 8a) and layer thickness (Fig. 3), *Lemna* with algae (Fig. 9a), and *Potamogeton* (Figs 8a,b & 9c). Because the NDVI is computed using wavelengths that can be obtained from most multispectral remote sensing devices, we extended our results to multispectral satellite imagery data using unsupervised classification of IKONOS imagery.

Spatial distribution of species and thickness of aquatic plant layers derived from IKONOS satellite imagery matched our field survey observations very well (Fig. 10). First, there are good matches to *Potamogeton* clusters in the south-west part of the impoundment (Fig. 10a). Since *Potamogeton* typically produces rhizomes and stays in fixed locations, the ability to identify *Potamogeton* is most easily verified. Next is the identification of the thick layer of floating *Lemna* and *Lemna* with algae that may have died or drifted downstream to accumulate near the dam (upper right edge of each panel in Fig. 10a–c). The thick *Lemna* accumulation identified along the impoundment perimeter in the IKONOS image further supports the interpretation based on remote sensing. Finally, this evidence correlates well with the generalized field observations of *Lemna* on the surface of the impoundment (Fig. 10b).

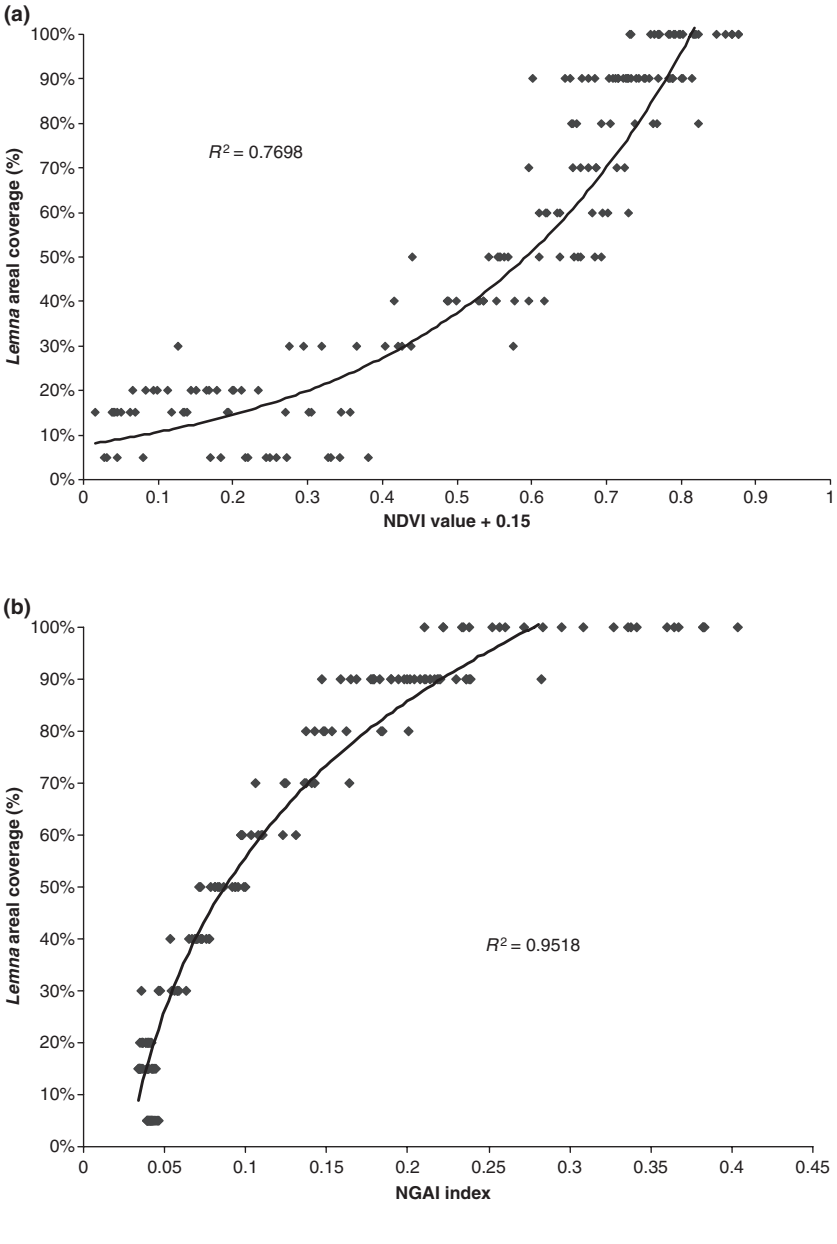

Fig. 7 Correlation between *Lemna* areal coverage and (a) NDVI; (b) NGAI.

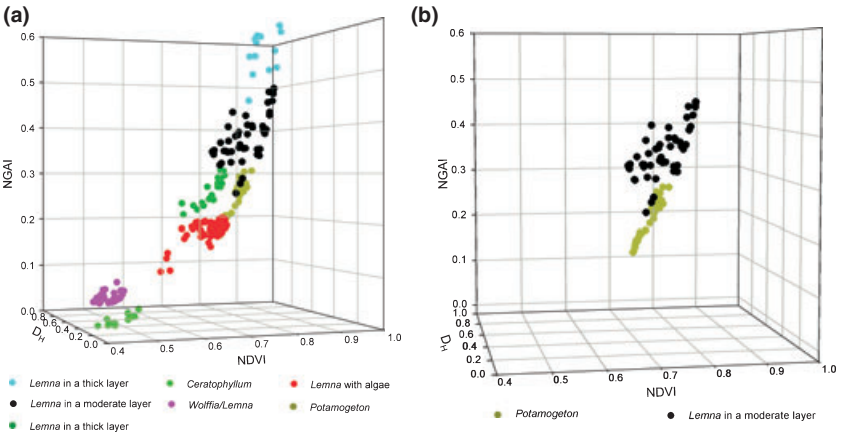

Fig. 8 Scatter plot graph of: (a) Seven major field-sample data classes in three-dimensional feature space of NGAI, NDVI, and D_H; (b) *Potamogeton* and *Lemna* in a moderate layer.

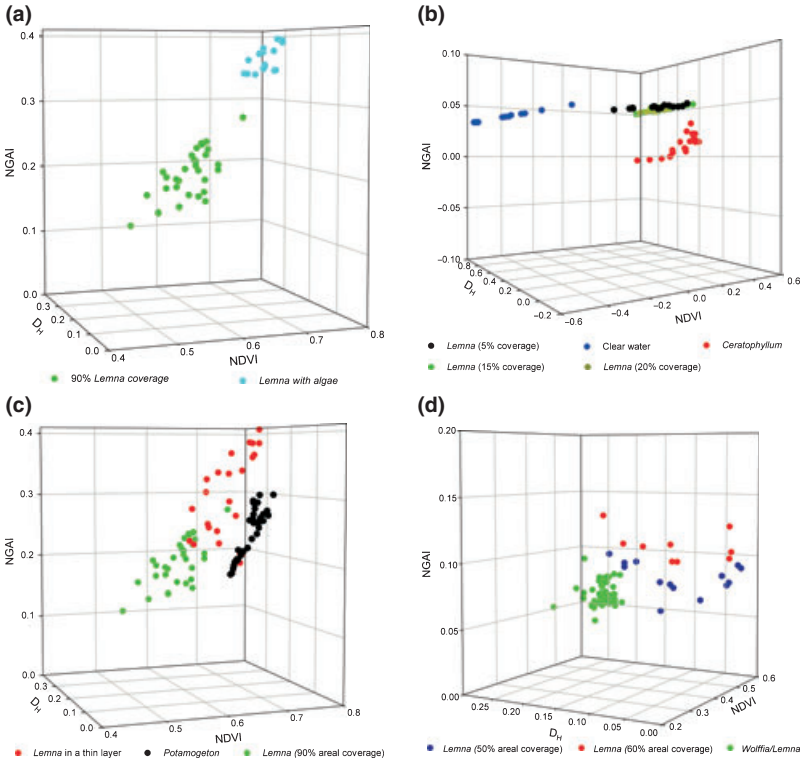

Fig. 9 Scatter plot graphs for resolving ambiguous field-sample data for four complex plant associations in three-dimensional feature space of NGAI, NDVI, and D_H; (a) *Lemna* with algae and *Lemna* (90% areal coverage); (b) *Ceratophyllum* and *Lemna* (5–20% areal coverage); (c) *Potamogeton* and *Lemna* (90–100% areal coverage); and (d) *Wolffia/Lemna* and *Lemna* (50–60% areal coverage).

To quantify the differences in areal coverage between the IKONOS-based classifications (Fig. 10a) and the four levels of visual observations of *Lemna* areal coverage as delineated in field-survey grids for the Ben Smith impoundment (Fig. 10b), we calculated the percentages of pixels covered by *Lemna*-dominated aquatic plants in the survey's individual cells. Then, using the ranges defined for field survey, the percentages were classified according to the four areal coverage levels (Fig. 10c). Differences between visually and remotely sensed cell classifications were compared graphically (Fig. 10d) and compiled in a confusion matrix (Congalton, 1991) (Table 2).

Discussion

This work demonstrates the identification and use of the unique features of the hyperspectral signatures of close assemblages of aquatic plant species typical of riverine habitats to adapt three vegetation indices useful in classifying. Further, the vegetation indices were applied to identify these heterogeneous plant groups from commercially available satellite imagery. Previous work on riverine systems has been limited by the availability of imagery with sufficient spatial and spectral resolution to work in river systems and by the difficulty of separating submerged plants from open water areas (Schweizer, Armstrong & Posada, 2005; and Gullstrom *et al*., 2006). Our data (Fig. 4a) show that at least in shallow, relatively clear impoundments, it is possible to distinguish submerged vegetation from open water. The combination of a library of hyperspectral signatures, adapted vegetation indices and pan-sharpened satellite imagery provides a strong set of tools for identifying and monitoring aquatic vegetation.

Field measurements and their interpretation

The large set of field samples examined here allowed the identification of unique spectral features for each assemblage of aquatic plants identified in the field. The hyperspectral signatures for the various floating plant distributions and assemblages are probably affected by a combination of the leaf morphology of each species, the varying internal moisture and chlorophyll content of healthy and dead plants in the mixture, and a combination of plant and water signatures (Malthus & George, 1997). The combined absorption effects of internal leaf structure of *Lemna*

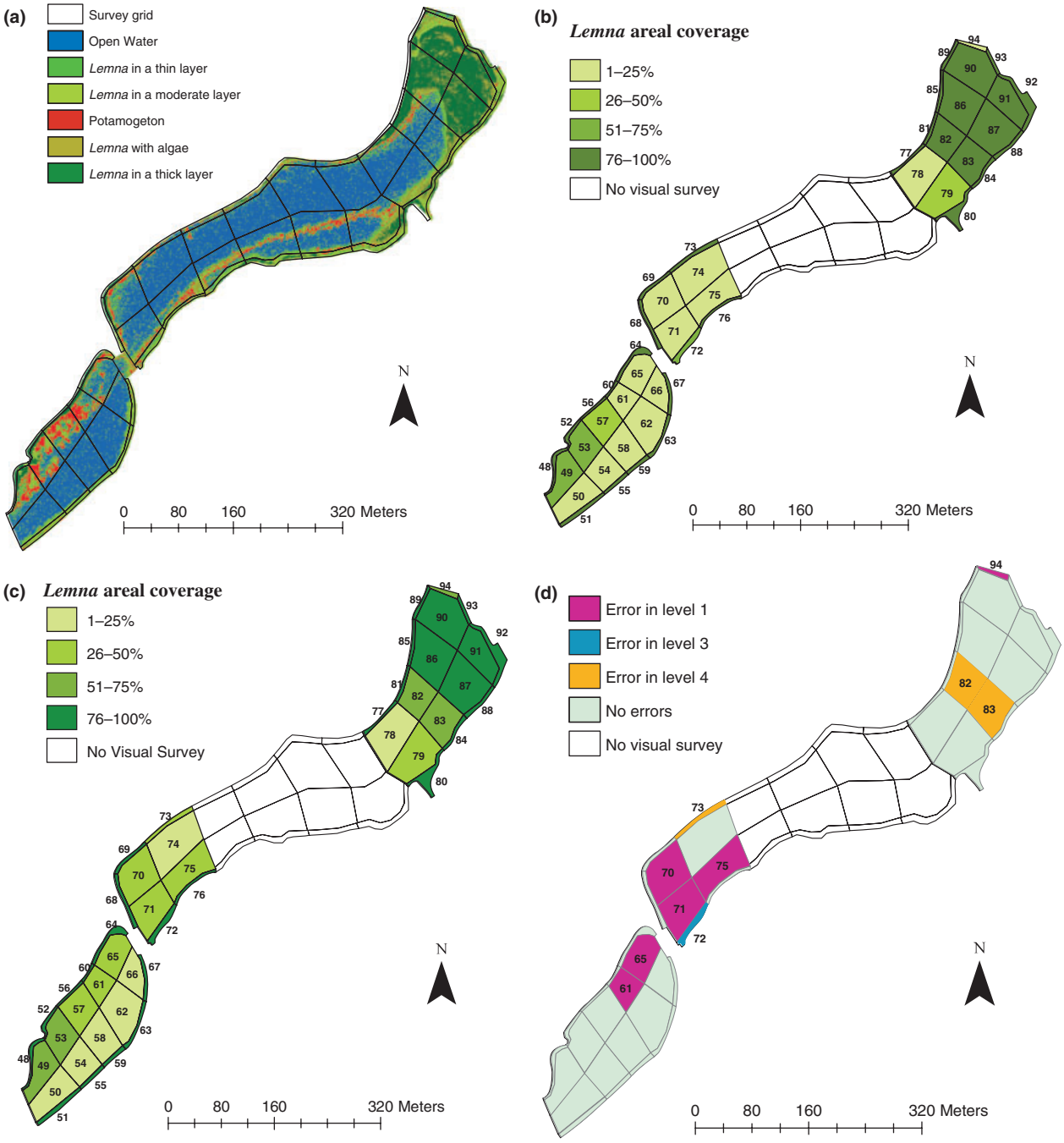

Fig. 10 Estimated aquatic plant distributions in Ben Smith impoundment visual survey area on 16 August 2007 using (a) unsupervised classification of IKONOS imagery; (b) visual observations in routine field survey; (c) remote sensing results classified according to the visual survey scale; and (d) discrepancies between remote sensing and visual surveys for each coverage level.

and open water between fronds are probably responsible for relatively low NIR reflectance in areas of sparse coverage (Fig. 3).

A number of specific hyperspectral features prove useful in resolving aquatic plant associations with similar spectral signatures (Fig. 5). For example, two spectral features help distinguish between *Lemna* with 90% areal coverage and *Lemna* with algae (Fig. 5a): (i) *Lemna* with algae absorbs more strongly at about 977 nm than *Lemna* at 90% areal coverage and (ii) the

Table 2 Accuracy assessment (confusion matrix) for the comparison of areal coverages using satellite and visual observation data

IKONOS result	Visual survey areal coverage				Total	Omission error %
	VS level 1	VS level 2	VS level 3	VS level 4		
RS level 1	**7**	0	0	0	7	0
RS level 2	5	**2**	0	1	8	38
RS level 3	1	0	**2**	2	5	60
RS level 4	0	0	1	**26**	27	4
Total	13	2	3	29	**47**	
Commission error %	46	0	34	10	Overall accuracy	
Correctly classified %	54	100	66	90	**79**%	

VS level$_i$, visual survey as level *i* areal coverage; RS level *i*, remote sensing as level *i* areal coverage.

R/NIR reflectance ratio for *Lemna* with algae is less than the ratio for *Lemna* at 90% areal coverage. Submerged plants and *Lemna* with 0–15% areal coverage also have similar spectra (Fig. 5b); however, the spectral signature of submerged plants has substantially higher reflectance in the NIR than in the red band, making differentiation possible. The leaves of *Potamogeton* and *Lemna* with 90–100% areal coverage are characterized by similar shapes and reflectance ranges of their spectral signature curves (Fig. 5c). The G/NIR reflectance ratio for *Potamogeton* differs from that of *Lemna* with an areal coverage from 90 to 100%. Furthermore, the slope of the common baseline between two local spectral maxima, at wavelengths 915 nm and 1073 nm, is positive for *Potamogeton* but not for the *Lemna* coverages. Integrating spectral features at three bands in the classification scheme – reflectance at the green and NIR bands and absorption at 977 nm – can be used to distinguish these two cases. Finally, moderate-density *Lemna* areal coverages (50–60%) and *Wolffia*-dominated *Wolffia/Lemna* associations could be differentiated by the rising slope for wavelengths from 750 to 915 nm in the *Wolffia/Lemna* signature.

Vegetation indices

The three vegetation indices, NGAI, NDVI and D_H derived from *in situ* hyperspectral samples proved effective in interpreting aquatic plant areal coverage, thickness of floating plant (*Lemna*) layers (thin, moderate and thick) and species composition (*Lemna*, *Lemna* with algae, *Wolffia/Lemna* and *Potamogeton*). The results from mapping aquatic plants with IKONOS multispectral imagery demonstrate that these data can be used to assess dense coverages of floating plants nearly as effectively as hyperspectral data.

Because of the minimal differences between the satellite-data-derived NDVI and the *in situ*-derived NDVI (Fig. 6), we were able to identify the three *Lemna* thickness levels with just the IKONOS NDVI values. Each of the two remaining classes, *Potamogeton* and *Lemna* with algae, had similar NDVI values. Fortunately, these two remaining classes occurred in different areas of the impoundment and, by referencing their spatial distributions, all remaining issues in assigning the five classes with appropriate biological and species information could be resolved by applying IKONOS data.

An increase in the NGAI value represents the increased spectral reflectance ratio of G/NIR and/or stronger absorption at 977 nm. In classifying the *Lemna* layers, the NDVI correlated linearly with the NGAI. The NDVI was effective at separating *Potamogeton* and *Lemna* in moderate thick layers, but the NDVI alone did not distinguish well the boundary overlaps between thin and moderate and between moderate and thick *Lemna* layers. The normalized absorption depth (D_H) was important for distinguishing between the *Wolffia/Lemna* association and *Ceratophyllum*. The D_H at the wavelength 977 nm allowed distinct differentiation between *Wolffia/Lemna* and *Ceratophyllum* and was also more effective than the other two indices at separating *Potamogeton* and *Lemna* in a moderate layer (Fig. 8b).

Because the NGAI integrates features of three wavelength bands, it has an advantage over the use of NDVI which uses two bands – red and NIR. On the other hand, although the use of the NDVI as a sole variable for estimating *Lemna* coverage is slightly less accurate than the NGAI, the NDVI is convenient to

use because most sensors, especially the high-resolution, multispectral sensors, such as IKONOS and QuickBird, provide red and NIR bands. Since high spatial resolution is extremely desirable for identifying heterogeneous associations of aquatic plants in river ecosystems, results from using the NDVI to estimate *Lemna* areal coverage from satellite-based remote sensing should prove invaluable. By combining the D_H with the NGAI and the NDVI for separating samples with mixed species associations and *Lemna* layer thicknesses, all seven scenarios in the *in situ* spectroradiometer measurements could be successfully grouped and identified with little ambiguity.

Satellite- versus observer-based assessments

The confusion matrix data (Table 2) show that overall agreement between satellite imagery and observer-based assessment methods was 79%. Agreement at level 4 (the greatest areal coverage) was the best (90%, or 26 out of 29 cells), which is important, because about 62% of the survey cells were designated as level 4. Almost all level 4 coverage cells were located near the dam and perimeter of the impoundment where *Lemna* and other drifting aquatic plants tend to accumulate under low-flow conditions. Two of the three differences between visual and remote sensing assessments at level 4 occurred in cells 82 and 83 (Fig. 10d). The *Lemna* coverages estimated from remote sensing at levels 2 and 3 agreed 100% and 66%, respectively, with the visual survey results. However, the results were based on small sample sizes at these two levels, and further testing may be required. The *Lemna* coverages in levels 2 and 3 were associated with 2 boundaries between coverage levels (for example, level 2 is bounded by levels 1 and 3). Thus, more disagreements between survey results and remote sensing results at these two levels than in level 1 and level 4 might be expected. If we adjust those discrepancies (in level 1 and level 4) between the routine visual assessment and the field observations described earlier, aquatic plant coverage resulted from remote sensing data can achieve an overall accuracy of 89%, a substantial improvement over the original results in Table 2.

There are several reasons for the differences between satellite- and observer-based visual coverage assessments: (i) the visual survey data may be described as semi-quantitative, narrative and/or subjective; the observer must estimate the percentage of each cell's surface area that would be covered with *Lemna* (and not considering other plant coverage) if any accumulations were distributed evenly across the cell's surface and, then, must assign the level of coverage; (ii) with remote sensing, it is difficult to distinguish very sparse *Lemna* coverages from open water (<25% coverage); (iii) given the drifting nature of *Lemna*, visual survey data can only rarely define a cell as 0% *Lemna* coverage, resulting in many cells being classified as 1–25% areal coverage; and (iv) differences were also, at least in part, because of the conversion between the percentage of coverage from the 1-m resolution remote sensing results and the visual categorical resolution of the field survey.

Future considerations

The remote sensing interpretations constitute an objective assessment of the true extent of aquatic plant distribution in this impoundment system and demonstrate the great potential for assessing *Lemna* density and other floating plant assemblages over a wide area. Using high-resolution satellite images, in general, yields more precise mapping coverage of floating aquatic plants over a wide area than land-based human observers can. The remote sensing results could probably be further improved by using a supervised classification scheme. Our field measurements and analysis can serve as an initial spectral library for a variety of aquatic plant species and associations prevailing in New England inland waters. Although not discussed here, our experience with obtaining timely satellite images suggests that on demand, airborne remote sensing may be a more practical option for assessing aquatic floating plants for entire water bodies in an acceptable timeframe.

Acknowledgments

The authors thank Prof. Roger Jones, Associate Editor, and two anonymous referees for their invaluable comments and suggestions on previous drafts of the manuscript. This study was supported, in part, by funding from the Massachusetts Department of Environmental Protection through a cooperative programme with the U.S. Geological Survey's

Massachusetts-Rhode Island Water Science Center. Use of a trade, product, or firm name is for descriptive purposes only and does not imply endorsement by the U.S. Government.

References

ASD Inc. (2008) FieldSpec® 3 User Manual. ASD Document 600540 Rev. H (http://www.asdi.com)

Baret F. & Guyot G. (1991) Potentials and limits of vegetation indexes for Lai and Apar assessment. *Remote Sensing of Environment*, **35**, 161–173.

Clark R.N. & Roush T.L. (1984) Reflectance spectroscopy – quantitative-analysis techniques for remote-sensing applications. *Journal of Geophysical Research*, **89**, 6329–6340.

Congalton R.G. (1991) A review of assessing the accuracy of classifications of remotely sensed data. *Remote Sensing of Environment*, **37**, 35–46.

Curcio J.A. & Petty C.C. (1951) The near infrared absorption spectrum of liquid water. *Journal of the Optical Society of America*, **41**, 302–304.

ERDAS (2003) *ERDAS Field Guide*. Leica GeoSystems, Atlanta.

Gullstrom M., Lunden B., Bodin M., Kangwe J., Ohman M.C., Mtolera M.S.P. & Bjork M. (2006) Assessment of changes in the seagrass-dominated submerged vegetation of tropical Chwaka Bay (Zanzibar) using satellite remote sensing. *Estuarine Coastal and Shelf Science*, **67**, 399–408.

Jacquemoud S. & Ustin S.L. (2003) Application of radiative transfer models to moisture content estimation and burned land mapping. In: *4th International Workshop on Remote Sensing and GIS Applications to Forest Fire Management* (Eds E. Chuvieco, P. Martin & C. Justice), pp. 3–12. Ghent, Belgium.

Jakubauskas M., Kindscher K., Fraser A., Debinski D. & Price K.P. (2000) Close-range remote sensing of aquatic macrophyte vegetation cover. *International Journal of Remote Sensing*, **21**, 3533–3538.

Jensen J.R. (2007) *Remote Sensing of the Environment: An Earth Resource Perspective*. Pearson Prentice Hall, Upper Saddle River, NewJersey.

Junk W.J. (1997) *The Central Amazon Floodplain: Ecology of a Pulsing System*. Springer, Berlin.

Khanna S., Palacios-Orueta A., Whiting M.L., Ustin S.L., Riano D. & Litago J. (2007) Development of angle indexes for soil moisture estimation, dry matter detection and land-cover discrimination. *Remote Sensing of Environment*, **109**, 154–165.

Kokaly R.F. & Clark R.N. (1999) Spectroscopic determination of leaf biochemistry using band-depth analysis of absorption features and stepwise multiple linear regression. *Remote Sensing of Environment*, **67**, 267–287.

Lillesaeter O. (1982) Spectral reflectance of partly transmitting leaves – laboratory measurements and mathematical-modeling. *Remote Sensing of Environment*, **12**, 247–254.

Malthus T.J. & George D.G. (1997) Airborne remote sensing of macrophytes in Cefni Reservoir, Anglesey, UK. *Aquatic Botany*, **58**, 317–332.

Marion L. & Paillisson J.M. (2003) A mass balance assessment of the contribution of floating-leaved macrophytes in nutrient stocks in an eutrophic macrophyte-dominated lake. *Aquatic Botany*, **75**, 249–260.

Nelson S.A.C., Cheruvelil K.S. & Soranno P.A. (2006) Satellite remote sensing of freshwater macrophytes and the influence of water clarity. *Aquatic Botany*, **85**, 291–300.

Nezlin N.P., Kamer K. & Stein E.D. (2007) Application of color infrared aerial photography to assess macroalgal distribution in an eutrophic estuary, upper Newport Bay, California. *Estuaries and Coasts*, **30**, 855–868.

Numata I., Roberts D.A., Chadwick O.A., Schimel J.P., Galvao L.S. & Soares J.V. (2008) Evaluation of hyperspectral data for pasture estimate in the Brazilian Amazon using field and imaging spectrometers. *Remote Sensing of Environment*, **112**, 1569–1583.

Palacios-Orueta A., Khanna S., Litago J., Whiting M.L. & Ustin S.L. (2006) Assessment of NDVI and NDWI spectral indices using MODIS time series analysis and development of a new spectral index based on MODIS shortwave infrared bands. In: *Proceedings of the 1st International Ionference of Remote Sensing and Geoinformation Processing* (ed. A. Roder & J. Hill), pp. 207–209. Trier, Germany.

Penuelas J., Gamon J.A., Griffin K.L. & Field C.B. (1993) Assessing community type, plant biomass, pigment composition, and photosynthetic efficiency of aquatic vegetation from spectral reflectance. *Remote Sensing of Environment*, **46**, 110–118.

Pu R., Ge S., Kelly N.M. & Gong P. (2003) Spectral absorption features as indicators of water status in Quercus Agrifolia leaves. *International Journal of Remote Sensing*, **24**, 1799–1810.

Rees W.G., Williams M. & Vitebsky P. (2003) Mapping land cover change in a reindeer herding area of the Russian Arctic using Landsat TM and ETM+ imagery and indigenous knowledge. *Remote Sensing of Environment*, **85**, 441–452.

Rouse J.W. Jr, Haas R.H., Schell J.A. & Deering D.W. (1974) *Monitoring the Vernal Advancement and Retrogradation (Green Wave Effect) of Natural Vegetation*. Prog. Rep. RSC 1978-1, Remote Sensing Center, Texas

A&M Univ., College Station, 93 p. (NTIS No. E73-106393).

Schweizer D., Armstrong R.A. & Posada J. (2005) Remote sensing characterization of benthic habitats and submerged vegetation biomass in Los Roques Archipelago National Park, Venezuela. *International Journal of Remote Sensing*, **26**, 2657–2667.

Silva T.S.F., Costa M.P.F., Melack J.M. & Novo E.M.L.M. (2008) Remote sensing of aquatic vegetation: theory and applications. *Environmental Monitoring and Assessment*, **140**, 131–145.

Stow D., Coulter L., Kaiser J., Hope A., Service D., Schutte K. & Walters A. (2003) Irrigated vegetation assessment for urban environments. *Photogrammetric Engineering and Remote Sensing*, **69**, 381–390.

(Manuscript accepted 11 January 2010)